Proc. of the 9th International Symposium on Geotechnical Safety and Risk (ISGSR)
Edited by Zhongqiang Liu, Jian Dai and Kate Robinson
Published by Research Publishing, Singapore.
doi: 10.3850/GRF-25280825_isgsr-224-P398-cd

NUMERICAL INVESTIGATION OF THE BAIGE LANDSLIDE-INDUCED WAVE PROPAGATION IN A NARROW RIVER CHANNEL

Hao Wu

College of Transportation Engineering, Nanjing Tech University, China. E-mail:wuhaogeot@njtech.edu.cn

Qing Cheng

School of Earth Sciences and Engineering, Nanjing University, China. E-mail:chengqing@nju.edu.cn

Abstracts:Landslide-induced waves pose significant risks to human life, property, and infrastructure, especially in relatively narrow channels where wave propagation differs from that in reservoirs or coastal areas. This study introduces a drift-flux model, treating the two-phase mixture as a whole to simulate flow-like landslide-induced waves efficiently. The model combines the renormalization group k<μ turbulence model and volume of fluid method to accurately describe wave formation and propagation. After verification through mesh size convergence tests and a benchmark experiment, the model is applied to the Baige landslide-induced waves in a narrow river channel on October 10, 2018. The results indicate that wave evolution occurs in four stages: run-up, inundation, run-down, and propagation along the valley. The run-up heights and wave decays vary between upstream and downstream locations at the same distance from the landslide center, depending on the extension direction of the river channel. The numerical predicted maximum run-up height of the Baige landslide-induced waves on the opposite hill slope is 112 m, consistent with the actual situation. However, the maximum run-up heights predicted by empirical equations are lower than both the actual and numerical simulated values due to the lack of consideration of multiple wave reflections in a narrow river channel. Utilizing the previous empirical equations to evaluate landslide-induced waves in a narrow river channel may result in underestimating their hazard. This study contributes to the risk assessment of landslide-induced waves in narrow water bodies, and its findings are essential for safety management and siting decisions regarding infrastructure and facilities.

Keywords: Baige landslide, impulse waves, narrow river channel, numerical simulation, run-up height

1. Introduction

Landslides are common geological phenomena in mountainous regions that can lead to impulse waves, barrier lakes, and other secondary effects, significantly endangering human life, property, and infrastructure (Cheng et al. 2024, Cui et al. 2009, Fritz et al. 2004, Li et al. 2024, Wu et al. 2020, Wu et al. 2023). A landslide-induced wave can directly damage residential areas, dams, and adjacent roads, railways, and bridges. Alaska experienced a massive landslide-induced wave on July 9, 1958, resulting in a colossal wave with a run-up height of 524 m (Fritz et al. 2009). The most well-known incident took place at the Vajont dam reservoir in Northern Italy, where an impulse wave with a run-up height of 250 m overtopped the dam, resulting in the loss of approximately 2000 lives (Rose and Hungr 2007, Xu et al. 2022). In the Three Gorges Reservoir in China, the Qianjiangping landslide-induced wave occurred on July 14, 2003, leading to 11 missing fishermen and the overturning of 22 fishing boats (Wang et al. 2017). Since 2008, landslide-induced waves have been frequently reported in the reservoir areas of the Three Gorges Reservoir in China, involving incidents such as the Gongjiafang landslide, the Qingshi landslide, and the Hongyanzi landslide, leading to numerous casualties and substantial financial losses (Yin et al. 2015). These events underscore the significance of comprehending landslide-induced wave propagation to facilitate preliminary hazard assessment and risk management.This work aims to provide guidance for the risk assessment of landslide-induced wave in a narrow river channel, with the following sub-aims:(a) Verify the effectiveness of the proposed numerical method;(b) Reproduce and investigate the Baige landslide-induced wave propagation in a narrow river channel;(c) Provide insight into the effect of the extension direction of river channel on the run-up height and wave decay of the impulse wave on the adjacent and opposite hill slopes.

2. Overview of the Baige landslide

Two successive landslides in Baige village, Tibet, Southwest China, on the right bank of the Jinsha River (31° 4′ 56.41″ N, 98° 42′ 17.98″ E), that occurred on October 10 and November 3, 2018, respectively, have aroused widespread concern in the landslide study community, and a number of studies have been reported so far (Li et al. 2023, Liu et al. 2021, Yan et al. 2022). When the second Baige landslide that occurred on November 3, 2018, the river channel still retained the deposits generated by the first landslide that occurred on October 10, 2018, so there was no obvious impulse wave in the second landslide. Thus, our study focused on the first landslide that occurred on October 10, 2018.

The valley where the landslide occurred exhibited a typical V-shaped morphology, with slope angles ranging from 30 to 50°. The Baige landslide mass primarily comprised fractured rock and gravel-soil, resulting

in a large wave when over 2.4×10^7 m^3 of landslide volume plunged into the narrow river channel. The main parameters of the Baige landslide, with an average width and thickness of approximately 600 m and 20 m, respectively. The highest elevation of the landslide area and the average free surface elevation of the Jinsha River were 3720 m a.s.l. and 2910 m a.s.l., respectively, resulting in a relative elevation difference of over 800 m (Hu et al. 2020). During the dry season, the valley's elevation ranged from 2850-2880 m a.s.l., with an average elevation of 2870 m a.s.l.

A field investigation showed that the maximum elevation of the Baige landslide-induced wave reaching the left bank of the Jingsha River was approximately 3040–3050 m a.s.l (Hu et al. 2020). On the left bank of the Jinsha River, observable effects of the landslide-induced wave include vegetation damage, extensive scattered debris, and scour marks (Hu et al. 2020).

3. Methods

The finite-volume CFD code Flow3D was used in the present study to model the Baige landslide-induced wave. The drift-flux model (DFM) was applied to model the interaction between landslide mass and water. The renormalized group model (RNG)-based k-epsilon turbulence model (k-μ) was employed to compute turbulence and viscosity problems.

In fluids composed of multiple elements, such as liquids and particles, the velocities of these components may vary. The primary cause of these velocity differences is typically non-uniform body forces resulting from density variations. Despite these differences, the relative velocities are generally small enough to be considered a "drift" between components under various conditions. This concept of "drift" is tied to the significance of the inertia of a dispersed element moving within another component. When the inertia of relative motion is negligible, a "drift-flux" model is used. In this approach, the relative velocity is minimized due to the balance between a pressure gradient and a counteracting drag force between the components. Drift velocities are crucial for the transport of both mass and energy.

A talus typically has a granular structure, which often results in circular failure surfaces during landslides. However, the findings from field observations, along with the topographical and geological characteristics of the Baige landslide study area, indicate that the failure surface in a talus may also be planar (Li et al. 2023). As a result, instead of sliding, a flowing movement could potentially occur, making the drift-flux model a suitable method for realistic simulation. In line with previous studies, the reservoir water is modeled as a fluid with a density of 1000 kg/m³, while the landslide material is treated as a fluid with a density of 1560 kg/m³. Therefore, the drift-flux model was applied in this study for analyzing two-phase flow dynamics.

The equation of continuous momentum balance of water can be written by Eq. (1), and the equation of momentum balance of solid flow can be written by Eq. (2) (Ersoy et al. 2022, Hibiki and Ishii 2003, Karahan et al. 2020).

$$\frac{\partial u_1}{\partial t}+u_1\cdot\nabla u_1=-\frac{1}{\rho_1}\nabla P+F+\frac{K}{f\rho_1}u_{\mathrm{r}} \quad (1)$$

$$\frac{\partial u_2}{\partial t}+u_2\cdot\nabla u_2=-\frac{1}{\rho_2}\nabla P+F-\frac{K}{(1-f)\rho_2}u_{\mathrm{r}} \quad (2)$$

where u_1 and u_2 indicate the velocities in a local grid cell of the continuous water phase and dispersed particle flow phase, respectively; ur denotes the difference in relative velocity between the two phases, which can be written by u_2-u_1; ρ_1 and ρ_2 denote the densities the continuous water phase and dispersed particle flow phase, respectively; P indicates fluid pressure; t denotes time; f is the volume fraction of the continuous water phase in the two-phase mixture; F denotes the body force; K denotes the drag coefficient associated with two phases interaction, which can be determined by the percentage of the two-phase mixture volume and the drag coefficient of the particle flow.

The drift flux model aims to compute the motion of the two phases relative to the volume-averaged velocity ($\bar{u}$). The volume-weighted average velocity is $\bar{u}=fu_1+(1-f)u_2$. The volume-weighted average velocity, chosen for its automatically enforced mass continuity, is preferred over the mass-weighted average. While some momentum may be transported, it is typically negligible and has been disregarded.

4. Evolution of the October 10, 2018 Baige landslide-induced wave

The velocity evolution of the two-phase mixture of the Baige landslide-induced wave, comprising the landslide and water, is illustrated in Fig. 1. At t = 8 s, the landslide commences, accompanied by the observation of tensile cracks in the trailing edge (Fig. 1a), influenced by gravity. By t = 15 s, the velocity at the landslide center reaches 50 m/s. Subsequently, the landslide's velocity diminishes, while the river's velocity increases, signifying the transfer of kinetic energy from the landslide to the river.

Stage one: From t = 18 s to 26 s, the waves surge up to the opposite hill, indicated by the velocity variation of reference point B.

Stage two: From t = 26 s to 36 s, the wave height at the opposite hill reaches its maximum. Stage three: From t = 37 s to 58 s, the velocity of reference point B first increases and then decreases, reflecting the waves and landslide running down from the opposite hill and subsequently depositing in the riverbed. Stage four: After the landslide impacts the narrow river channel, reference points A and C acquire velocity, signifying the propagation of the landslide-induced wave along the river (Fig. 1d).

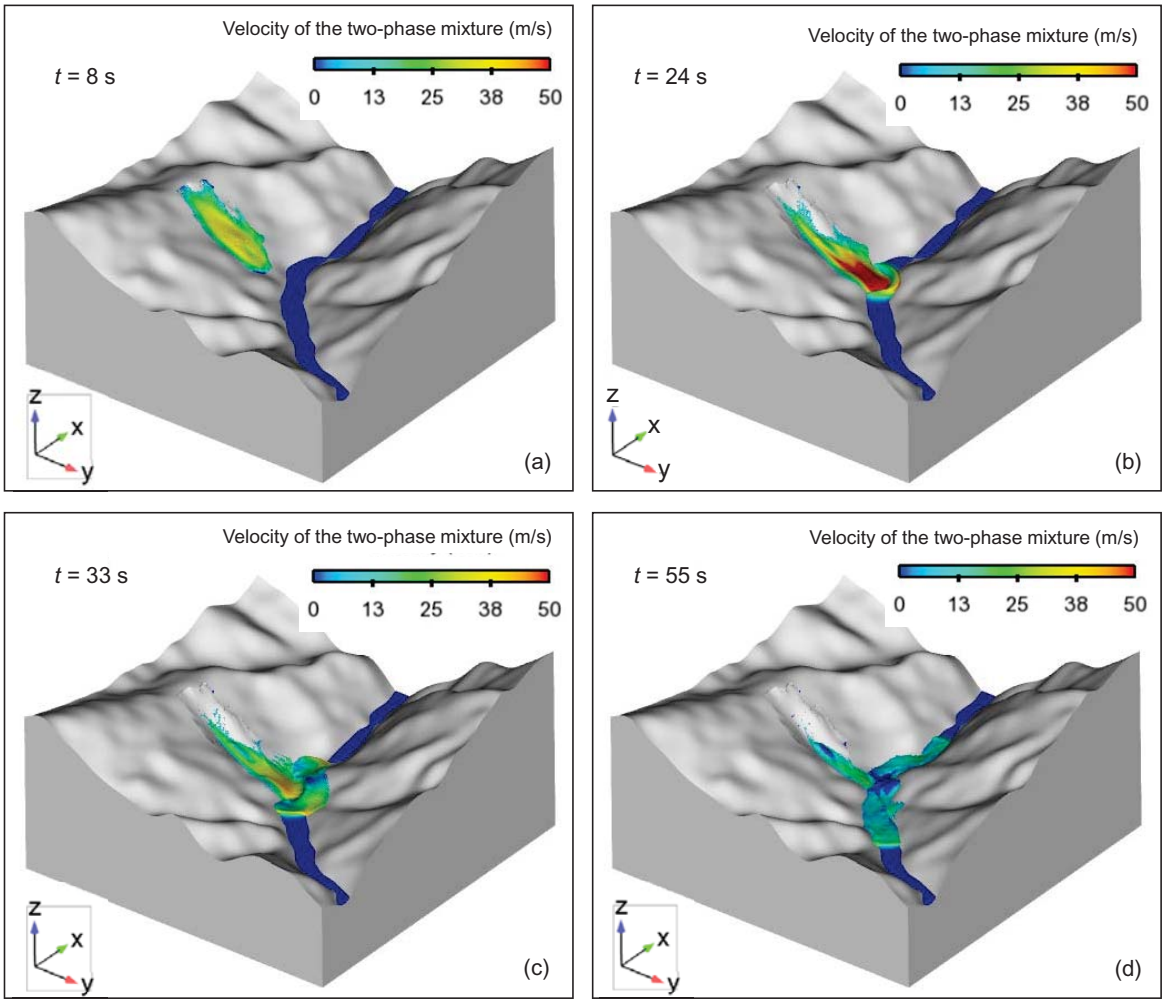

Fig. 1 The velocity evolution of the two-phase mixture of landslide and water of the Baige landslide-induced wave at different times. (a) t = 8 s; (b) t = 24 s; (c) t = 33 s; (d) t = 55 s.

5. Conclusions

Landslide-induced waves can bring catastrophic consequences. In this study, the drift-flux model is introduced to model the landslide-induced wave propagation in a narrow river channel. The following significant results are obtained:

(1) The evolution of the impulse wave in a narrow river channel can be divided into four stages: wave run-up, inundation, run-down on the opposite hill slope, and wave propagation along the valley. The lateral wave propagating along the narrow river channel undergoes wave superposition and attenuation processes, while the wave propagation energy at the opposite hill slope decreases along the valley.

(2) The runout distance of the wave along the narrow river channel is more than 2900 m, more than twice of that of the Baige landslide, indicating that the impact damage of the landslide-induced wave is greater than that of the landslide mass. The run-up heights and wave decays on the adjacent and opposite slopes of the Baige are different between upstream and downstream at the same distance from the landslide center. This suggests that a river channel's extension direction influences the run-up heights and wave decay of an impulse wave.

(3) Four well-known empirical models for predicting maximum run-up height of landslide-induced wave are compared with the numerical model. The predicted maximum run-up heights by the empirical models are much

smaller than the actual and numerically simulated values due to the lack of consideration of multiple wave reflections in a narrow river channel. Hence, using previous empirical equations to evaluate landslide-induced waves in a narrow river channel may underestimate its hazard.

Acknowledgement

This research was supported by the National Key Research and Development Program of China (2022YFC3080100), the National Natural Science Foundation of China (42207228), and the Sichuan Science and Technology Program (2022NSFSC1060).

References

Cheng Q, Gu YD, Tang CS, Zhang XY and Shi B (2024) Desiccation cracking behaviour of a vegetated soil incorporating planting density. Canadian Geotechnical Journal 61: 165-173.

Cui P, Zhu Y, Han Y, Chen X and Zhuang J (2009) The 12 may wenchuan earthquake-induced landslide lakes: Distribution and preliminary risk evaluation. Landslides 6: 209-223.

Ersoy H, O•uz Sünnetci M, Karahan M, Perinçek D (2022) 3D simulations of impulse waves originating from concurrent landslides near an active fault using FLOW-3D software: A case study of Çetin dam reservoir (Southeast Turkey). BullEng Geol Environ 81: 267.

Fritz HM, Hager WH and Minor HE (2004) Near field characteristics of landslide generated impulse waves. 130: 287-302.

Fritz HM, Mohammed F and Yoo J (2009) Lituya bay landslide impact generated mega-tsunami 50 th anniversary. Tsunami science four years after the 2004 indian ocean tsunami, Springer, pp 153-175

Hibiki, T., Ishii, M., 2003. One-dimensional drift–flux model for two-phase flow in a large diameter pipe. Int J Heat Mass Tran46 (10), 1773-1790.

Hu YX, Yu ZY, Zhou JW (2020) Numerical simulation of landslide-generated waves during the 11 October 2018 Baige landslide at the Jinsha River. Landslides 17, 2317–2328.

Karahan M, Ersoy H, Akgun A (2020) A 3D numerical simulation-based methodology for assessment of landslide-generated impulse waves: A case study of the Tersun Dam reservoir (NE Turkey). Landslides 17: 2777-2794.

Li Y, Cui Y, Hu X, Lu Z, Guo J, Wang Y, Wang H, Wang S and Zhou X (2024) Glacier retreat in eastern himalaya drives catastrophic glacier hazard chain. Geophysical Research Letters 51: e2024GL108202.

Li DY, Nian TK, Tiong RLK, Shen Y, Shao Z (2023) River blockage and impulse wave evolution of the Baige landslide in October 2018: Insights from coupled DEM-CFD analyses. Eng Geol321, 107169.

Liu D, Cui Y, Wang H, Jin W, Wu C, Bazai NA, Zhang G, Carling PA, Chen H (2021) Assessment of local outburst flood risk from successive landslides: Case study of baige landslide-dammed lake, upper jinsha river, eastern tibet. J Hydrol 599: 126294.

Rose ND and Hungr O (2007) Forecasting potential rock slope failure in open pit mines using the inverse-velocity method. International Journal of Rock Mechanics and Mining Sciences 44: 308-320.

Wang Y, Liu J, Li D and Yan S (2017) Optimization model for maximum tsunami amplitude generated by riverfront landslides based on laboratory investigations. Ocean Engineering 142: 433-440.

Wu H, Nian T, Chen G, Zhao W and Li D (2020) Laboratory-scale investigation of the 3-D geometry of landslide dams in a u-shaped valley. Engineering Geology: 105428.

Wu H, Nian T and Shan Z (2023) Investigation of landslide dam life span using prediction models based on multiple machine learning algorithms. Geomatics, Natural Hazards and Risk 14: 2273213.

Xu W, Zhou Q and Dong X (2022) SPH–DEM coupling method based on gpu and its application to the landslide tsunami. Part ii: Reproduction of the vajont landslide tsunami. Acta Geotechnica 17: 2121-2137.

Yin Y, Huang B, Chen X, Liu G and Wang S (2015) Numerical analysis on wave generated by the Qianjiangping landslide in three gorges reservoir, china. Landslides 12: 355-364.

Yan Y, Cui Y, Huang X, Zhou J, Zhang W, Yin S, Guo J and Hu S (2022) Combining seismic signal dynamic inversion and numerical modeling improves landslide process reconstruction. Earth Surf Dynam 10: 1233-1252.